Graphene Exfoliation at a Ferroelectric Domain Wall Induced by the Piezoelectric Effect: Impact on the Conductance of the Graphene Channel

Anna N. Morozovska,[1,2] Anatolii I. Kurchak,[3] and Maksym V. Strikha[3,4,*]

[1]*Institute of Physics, National Academy of Sciences of Ukraine, Prospect Nauky 46, 03028 Kyiv, Ukraine*
[2]*Bogolyubov Institute for Theoretical Physics, National Academy of Sciences of Ukraine, 14-b Metrolohichna Street, 03680 Kyiv, Ukraine*
[3]*V. Lashkariov Institute of Semiconductor Physics, National Academy of Sciences of Ukraine, Prospect Nauky 41, 03028 Kyiv, Ukraine*
[4]*Taras Shevchenko Kyiv National University, Radiophysical Faculty Prospect Akademika Hlushkova 4g, 03022 Kyiv, Ukraine*

(Received 10 June 2017; revised manuscript received 15 September 2017; published 3 November 2017)

p-n junctions in graphene on ferroelectric substrates have been actively studied, but the impact of the piezoelectric effect in ferroelectric substrate with ferroelectric domain walls (FDWs) on graphene characteristics was not considered. Because of the piezoeffect, ferroelectric domain stripes with opposite spontaneous polarizations elongate or contract depending on the polarity of voltage applied to the substrate. We show that the alternating piezoelectric displacement of the ferroelectric domain surfaces can lead to the alternate stretching and separation of graphene areas at the steps between elongated and contracted domains. Graphene separation at FDWs induced by the piezoeffect can cause unusual effects. In particular, the conductance of the graphene channel in a field-effect transistor increases significantly because electrons in the stretched section scatter on acoustic phonons. At the same time, the graphene conductance is determined by ferroelectric spontaneous polarization and varies greatly in the presence of FDWs. The revealed piezomechanism of graphene conductance control is promising for next generations of graphene-based field-effect transistors, modulators, electrical transducers, and piezoresistive elements. Also, our results propose the method of suspended graphene fabrication based on the piezoeffect in a ferroelectric substrate that does not require any additional technological procedures.

DOI: 10.1103/PhysRevApplied.8.054004

I. INTRODUCTION

Experimental and theoretical studies of the remarkable electromechanical, electrophysical, and transport properties of graphene remain a focus of researchers' attention since graphene's discovery [1,2] until now [3–5]. Despite prominent advances in understanding the complex physical processes taking place in graphene and other 2D semiconductors, these materials are not commercially used in modern electronic techniques despite very attractive application possibilities. Most challenges associated with the practical usage of these materials critically depend on the successful choice of electromechanical, electrophysical, and physicochemical properties of their environment (substrates, matrices, or gates). The environment should be compatible with a given 2D material and desirable to have additional degrees of functionality [3,6].

A promising and quite feasible way towards the commercialization of graphene-based devices (as well as devices utilizing other 2D semiconductors) is to use "smart" substrates with additional (electromechanical, polar, and/or magnetic) degrees of functionality, which are coupled with graphene. Of particular interest is a graphene on a ferroelectric substrate [7–11], whose spontaneous polarization and domain structure can be controlled by an external electric field [7–6,12,13]. For example, the polar state of a ferroelectric substrate can be readily switched by the voltage applied to the gate of the graphene field-effect transistor (GFET) [6,7], where a graphene or other 2D semiconductor sheet is a channel.

The presence of a domain structure in a ferroelectric substrate can lead to the formation of *p-n* junctions in graphene [12,13]. The junctions are located near the contact of the domain walls with the ferroelectric surface [14–16]. Note that the unique properties of the *p-n* junction in graphene have been realized much earlier by multiple gate doping of the graphene channel by electrons or holes, respectively [17–19]. Then they have been studied theoretically [20,21] and experimentally [22–24]. However, only relatively recently, Hinnefeld *et al.* [12] and Baeumer *et al.* [13] explored the advantages of creating a *p-n* junction in graphene using ferroelectric substrates. Notably, this way imposes graphene on a 180° ferroelectric domain wall (FDW). Because of the charge separation by an electric field of a FDW surface junction [25,26], a *p-n* junction can occur

*Corresponding author.
maksym.strikha@gmail.com

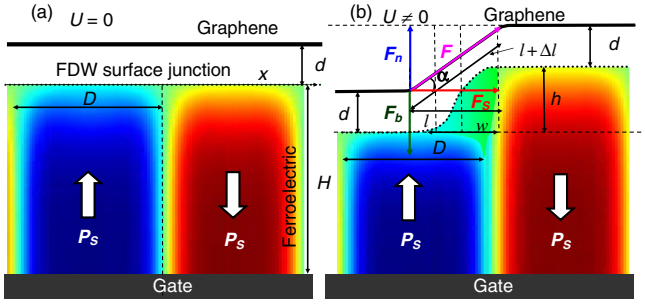

FIG. 1. Partial separation of graphene channel sections induced by a piezoelectric effect at the ferroelectric domain-wall surface junction. The separation is absent at $U = 0$ (a) and appears at $U \neq 0$ (b). In plot (b), F is the elastic tension force, F_n is its normal component, F_S is its lateral component, and F_b is the binding force of the carbon atom to the surface.

without any additional gate doping. Later on, semiquantum and semiphenomenological analytical models were developed for different types of carrier transport (ballistic, diffusive, etc.) in a single-layer graphene channel at 180° FDW [14,15]. The dynamics of p-n junctions in a graphene channel induced by FDW motion have been studied [16].

To the best of our knowledge, all existing theoretical models considering electrotransport in graphene on a ferroelectric substrate with FDWs do not consider the impact of the piezoelectric effect in the substrate on graphene strain (see, e.g., Refs. [14–16,20,21,25,26]). However, it is well known that the elastic strain can change the band structure of graphene (e.g., via the deformation potential) and open the band gap [4,5,27–29]. As we show in this paper, the elastic strain can significantly affect the graphene conductance via the *stretching* of its surface and *separation* of graphene areas at the steps between elongated and contracted domains.

The estimates made on the back of the envelope show that if the voltage U is applied to a gate of the GFET with FDW, one domain elongates and another one contracts depending on the voltage polarity [compare Fig. 1(a) with 1(b)]. The corresponding surface displacement can be significant for ferroelectrics with high piezoelectric coefficients. For instance, the piezoelectric coefficients of $PbZr_{0.5}Ti_{0.5}O_3$ (PZT) substrate can reach 0.3–1 nm/V depending on the film thickness and temperature [30]. Hence, the piezoelectric effect in PZT leads to its surface displacement $h \sim 0.5$–1 nm for the gate voltage of approximately 1–3 V. The thickness $d \leq 0.5$ nm of the physical gap between the graphene and ferroelectric is determined by van der Waals interaction. The density J of binding energy for graphene on SiO_2 substrate is about 0.5 J/m^2 [31]. Because graphene adhesion to a mica surface is considered to be the strongest one in comparison with other surfaces, it is natural to expect that the J value for graphene on a PZT surface is smaller. The Young's modulus of graphene is extremely high ($Y = 1$ TPa [32,33]) in comparison with other semiconducting solids.

Note that the height h of the ferroelectric surface displacement step induced by the piezoelectric effect at FDWs is usually much smaller than their width w [see designations in Fig. 1(b)], since, typically, $h \leq 1$ nm and $w \geq 5$ nm [34]. If the step width w is small enough in comparison with the domain size D, we can say that the displacement of the ferroelectric surface at FDW has a *"sharp profile"*. Under these conditions, the partially separated graphene region can occur at the step. This happens when the normal component F_n of the elastic tension force F applied to a carbon atom exceeds the force F_b binding the atom with the surface [see the scheme of the forces in Fig. 1(b)]. The separated section of length $l + \Delta l$ is "*suspended*" between the bounded sections. Its horizontal projection has length l, so that the small difference $\Delta l \ll l$ can be neglected since the height $h \ll w$ and, typically, $l \geq w$ [see designations in Fig. 1(b)]. For observable graphene separation, we require $D > (2\text{–}3)w$ (or even $D \gg w$).

Therefore, it makes sense to analyze more rigorously the piezoelectric displacement of a ferroelectric surface in the vicinity of the FDW surface junction. The analysis is presented below.

II. PIEZOELECTRIC DISPLACEMENT OF FERROELECTRIC SUBSTRATE SURFACE

Let us analyze the vertical displacement $u_3(x)$ of a ferroelectric film surface in the vicinity of the FDW surface junction induced by the piezoelectric effect. The voltage U is applied to the gate electrode. The analytical expression for $u_3(x)$ is derived in Ref. [34] within the framework of the decoupling approximation that is widely used for the piezoelectric response calculations [35–38]. The displacement $u_3(x)$ acquires the form [34]

$$u_3(x) = -U\left[W_{33}(x)d_{33} + W_{31}(x)d_{31}\right]. \qquad (1)$$

Here, U is the potential difference between the top and bottom electrodes, i.e., the gate voltage. Constants d_{33} and d_{31} are piezoelectric coefficients. They are temperature-dependent constants for thick ferroelectric films and tabulated for the bulk materials.

The presence of the first term proportional to d_{33} in Eq. (1) is anticipative because the spontaneous strain in the bulk of the ferroelectric with the spontaneous polarization P_3 is proportional to d_{33}. The origin of the second term proportional to d_{31} in Eq. (1) depends on the mechanical boundary conditions between the ferroelectric film and the gate electrode. The concrete forms of $W_{33}(x)$ and $W_{31}(x)$ are dictated by the conditions of the film and substrate electrode mechanical compatibility. Note that the ferroelectric film and gate electrode have close mechanical properties in a realistic situation of perovskite-on-perovskite epitaxial growth (e.g., for the pair $PbZr_xTi_{1-x}O_3$ on metallic $SrRuO_3$). Assuming that the mechanical properties of the film and electrode are

close, we can use the rigorous derivation of the terms in Eq. (1) presented in Ref. [34]. For this case, the functions W_{33} and W_{31} are

$$W_{33}(x)=\frac{2}{\pi}\left[\left(\frac{d}{H}+1\right)\arctan\left(\frac{x}{d+H}\right)-\left(\frac{d}{H}\right)\arctan\left(\frac{x}{d}\right)\right]+\frac{2}{\pi}\frac{x}{H}\ln\left(\frac{(d+H)^2+x^2}{d^2+x^2}\right), \quad (2)$$

$$W_{31}(x)=\frac{2(1+2\nu)}{\pi}\left[\left(\frac{d}{H}+1\right)\arctan\left(\frac{x}{d+H}\right)-\left(\frac{d}{H}\right)\arctan\left(\frac{x}{d}\right)\right]+\frac{\nu}{\pi}\frac{x}{H}\ln\left(\frac{(d+H)^2+x^2}{d^2+x^2}\right). \quad (3)$$

Here, H is the thickness of the ferroelectric film, d is the distance between the flat surface of ferroelectric and graphene, and v is the Poisson ratio [39]. Since the distance d is defined by the van der Waals forces, it is typically small (not more than 1 nm) [3], and so Eqs. (1)–(3) can be simplified in the limit $d \to 0$ (see Appendix A).

Notably, finite size effects and imperfect screening conditions (such as physical gaps [40] between the film and graphene and/or dead layers [41] near the ferroelectric surface) can strongly decrease the value of the spontaneous polarization in thin films. The effects eventually lead to the size-induced phase transition to a paraelectric phase with the film thickness decrease below the critical thickness H_{cr}. The critical thickness H_{cr} depends on the gap and/or dead layer thickness in a self-consistent way and usually does not exceed 5–15 nm for ultrathin gaps (see, e.g., Refs. [42,43]). As a result, the piezoelectric coefficients d_{33} and d_{31} included in Eqs. (1) and (3) and the next equations are no more constants defined for the bulk material but become polarization dependent. In the simplest case, the changes can be estimated from the expression $d_{ijk}=2\epsilon_0(\epsilon^f_{km}-\delta_{km})Q_{ijml}P^S_l$, where P^S_l are the components of spontaneous polarization, ϵ^f_{km} are components of relative dielectric permittivity tensor, and Q_{ijml} are the components of electrostriction tensor. On the other hand, the dead layer thickness H_{DL} and graphene-surface separation d contribute additively to the critical thickness, namely, $H_{cr} \sim H_{DL}+d$ [44]. The self-consistent problem of the d_{ijk} determination becomes analytically tractable for ultrathin gaps and dead layers (smaller than one to two lattice constants of ferroelectric and much smaller than the film thickness H) and enough thick films ($H \gg H_{cr}$) only. Based on the numerical results presented in Refs. [16,43], we can conclude that if the strong inequalities $H \gg H_{DL}+d$ and $H \gg H_{cr}$ are valid, one can regard P^S_l, d_{33}, and d_{31} equal to their tabulated values for a bulk material.

Figure 2 illustrates the profiles of the surface displacement calculated from Eqs. (1) and (2) at gate voltage $U = 1$ V, thermodynamic piezoelectric coefficients $d_{33} \approx 10^3$ pm/V and $d_{31} \approx -450$ pm/V, and Poisson ratio $v \approx 0.3$ corresponding to PZT at room temperature [30]. The values of the PZT film thickness H and distance d vary in the range $H = 20$–500 nm and $d = 0$–0.5 nm, respectively. Note that the vertical picometer scale is much smaller than the horizontal nanometer scale in Fig. 2.

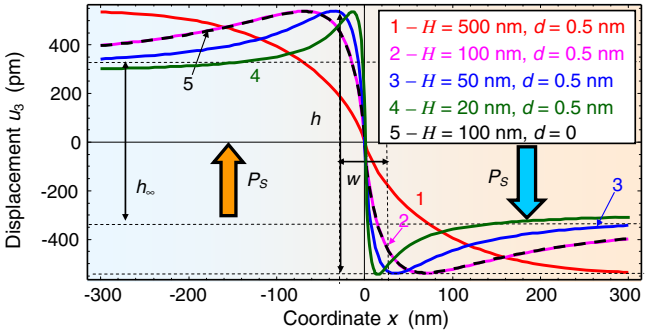

FIG. 2 Profiles of the ferroelectric surface displacement u_3 calculated from Eqs. (1)–(3) at the gate voltage $U = 1$ V, thermodynamic piezoelectric coefficients $d_{33} \approx 10^3$ pm/V, $d_{31} \approx -450$ pm/V, and Poisson ratio $v = 0.3$ corresponding to PZT at room temperature. The values of ferroelectric film thickness H and distance d for curves 1–4 are indicated in the legend. The step height h and width w for curve 3 are shown by vertical and horizontal arrows, respectively.

One can see from Fig. 2 that the step originated at the FDW surface junction is the widest for the smallest ratio d/H (curve 1 has a half-width of about 250 nm) and becomes significantly thinner with the ratio increase (curves 2–5 have a half-width of about 5–50 nm). The dashed curve 5 calculated for $d = 0$ and $H = 100$ nm is almost indistinguishable from curve 2 calculated for $d = 0.5$ nm and $H = 100$ nm. Hence, the step width is not defined by the ratio d/H only. It appears proportional to both of these values. Actually, the full step width w defined as the distance between its maximal positive and negative displacement (shown by a horizontal arrow in Fig. 2) can be estimated from the expression

$$w \approx k(H+d), \quad (4)$$

where the numerical factor k depends on the ratio d/H and appears smaller than unity for curves 2–5 shown in Fig. 2.

The step maximal height h changes in a nonmonotonic way with the d/H ratio increase, but the displacement difference is the same for all curves far from the domain wall. Actually, far from the wall $x \to \pm\infty$, functions $W_{3i}(x)$ in Eqs. (2) and (3) tend to ± 1. Hence, the "saturated" step height $h_\infty = |u_3(x \to \infty) - u_3(x \to -\infty)|$ is

$$h_\infty = 2|U|[d_{33}+(1+2\nu)d_{31}]. \quad (5)$$

The value h_∞ is independent of the ferroelectric thickness and proportional to the product of the gate voltage

and the combination of the piezoelectric coefficients $d_{33} + (1 + 2\nu)d_{31}$.

For the case $d \ll H$, the graphene stretching (without separation) can be favorable in the case of its contact with thick ferroelectric films characterized by smooth displacement profiles across the FDWs (see curve 1 in Fig. 2).

Note that the situation shown in Fig. 2 corresponds to an artificial case of a single domain wall in a ferroelectric film. In reality, ferroelectric films (of thickness less than dozens of microns) inevitably split into stripe domains if their surfaces are not in a perfect electric contact with ideally conducting electrodes [45,46]. The domain splitting occurs due to the long-range nature of the depolarization electric fields [46]. The incomplete surface screening of ferroelectric polarization strongly influences the domain nucleation and growth dynamics, domain-wall structure, and period in thin films under incomplete screening conditions [46]. The conditions are open-circuit electric boundary conditions [46,47], imperfect electrodes [48], separation from the electrodes by ultrathin dead layers [40], or spatial gaps [41]. Since the graphene layer is separated from the ferroelectric surface by the ultrathin gap of thickness d (see Figs. 1 and 3), the domain splitting can occur. So, the question about the relationship between the domain period and film thickness should be considered. In the simplest Kittel-type models, the period of domain stripes D with infinitely thin walls depends on the film thickness H in accordance with the Kittel-Mitsui-Furuichi (KMF) relation [46,49] $D = 2\sqrt{h_M H}$, where the length $h_M \cong A\epsilon_0(1 + \sqrt{\epsilon_{11}\epsilon_{33}})\psi_{DW}/P_S^2$ depends on the concrete model and ferroelectric parameters. The numerical coefficient $A \geq 3.7$, surface energy of the FDW $\psi_{DW} \sim (0.1 - 0.5)$ J/m^2, effective dielectric permittivity $\sqrt{\epsilon_{11}\epsilon_{33}} \sim (10^2 - 10^3)$, and spontaneous polarization $P_S \sim$ (0.05–0.5) C/m^2 depend on the film thickness and temperature. Estimates show that h_M appears about 1–10 nm, e.g., for $PbTiO_3$ at room temperature [43]. Notably, the KMF law $D \sim \sqrt{H}$ appears invalid for LGD-type models, which naturally accounts for FDWs broadening near ferroelectric surfaces separated by the gap from the conductor [43]. In numbers, the domain period D significantly increases with the screening degree increase reaching hundreds of nanometers for the ultrathin gap $d \sim 0.5$ nm used in this work. Therefore, the strong inequality $D \gg w$ is possible even in relatively thin films. Another challenge for the experimental situation presented in Figs. 1 and 3 is how to prevent the uncontrollable motion and splitting of the separated FDWs in thin films under the gate-voltage increase. However, lattice potential and defects pin the walls rather strongly (see Chap. 8, Sec. 8.5 in Ref. [42] and references therein, as well as Refs. [50–53]).

III. PIEZOELECTRIC EFFECT IMPACT ON THE GRAPHENE LAYER

The complete separation (i.e., exfoliation) of graphene caused by a piezoelectric effect is hardly possible in thick

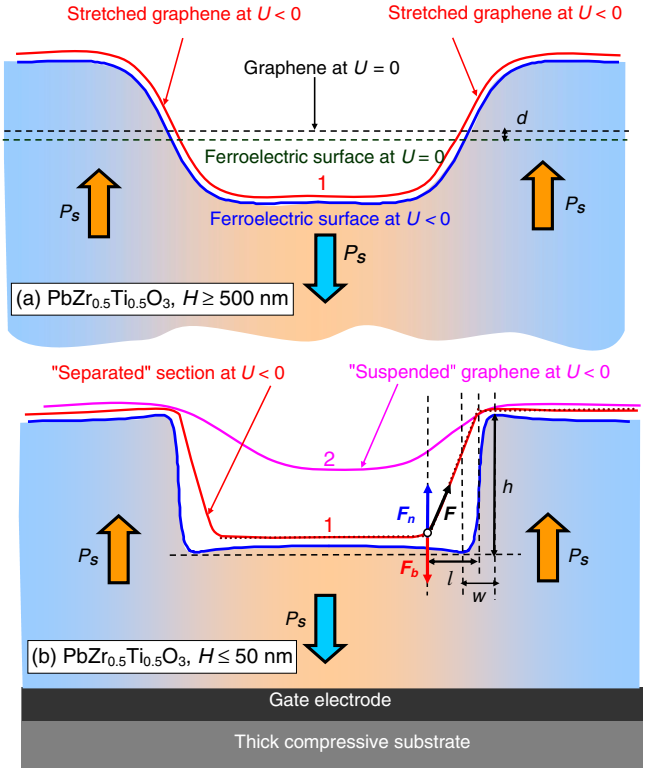

FIG. 3 Schematic profiles of the ferroelectric film and graphene-surface displacements for $U = 0$ (dashed horizontal lines) and $U < 0$ (solid curves 1, 2). (a) Graphene stretching (without any separation) induced by the piezoelectric effect in thick films with smooth profile of the surface displacement across the FDWs (red curve 1). (b) Partial (red curve 1) and complete (magenta curve 2) separation of the graphene region induced by the piezoelectric effect in thin films with sharp profile of the surface displacement across the FDWs. Note that vertical scale is much smaller than the horizontal one and so $l \gg h$ (see Fig. 2 for clarity).

ferroelectric films with smooth profiles of the surface displacement ($w \sim D$) corresponding to curve 1 in Fig. 2. The complete exfoliation becomes impossible if the domain wall is a single one in a film, and so only the stretching of graphene sheet is induced by the piezoelectric effect in this case. The typical picture of graphene stretching by a piezoelectric effect in a thick film is shown in Fig. 3(a).

The partial separation or complete exfoliation of graphene can be favorable when it contacts with relatively sharp ferroelectric surface profiles across the FDWs ($w \ll D$) corresponding to curves 2–5 in Fig. 2. A typical picture of graphene partial separation or complete exfoliation caused by a piezoelectric effect in a thin film is shown in Fig. 3(b) by solid red and magenta curves, respectively. The separated sections are suspended and fixed between the bounded graphene regions. The stretching of the suspended graphene regions can be strong enough in the case of its partial fixing by the ferroelectric surface [see the red curve

1 in Fig. 3(b)] if the van der Waals forces can hold the graphene at the bottom of the cavities induced by the piezoelectric effect on the domain structure. Note that the graphene stretching is almost absent in the case of its complete exfoliation from the ferroelectric surface due to the weakness of the van der Waals forces, and the graphene sheet is suspended above the bottoms of the domains walls in this case [see magenta curve 2 in Fig. 3(b)].

Which case (stretching, partial separation, or complete exfoliation) can be realized in a real system? Only self-consistent numerical calculations of the elastic subproblem allowing for *ab initio* calculations of the binding energy J and distance d can give the answer to this question. Unfortunately, the calculations being beyond the scope of this work are absent to date. Hence, all possible cases of graphene mechanical behavior can be realized for a given piezoelectric displacement of the ferroelectric film surface.

Thus, depending on the ratios D/H and d/h, the situation with graphene stretching and partial separation can be very different (see Fig. 3). Taking into account the warning, the length of the graphene section separated from the ferroelectric surface can be estimated for the sharp profile of the surface displacement; the graphene-surface profile is approximated by dotted lines in Fig. 3(b). The limits for this model applicability are discussed later. It is natural to expect that the graphene separation occurs right to the point, where the normal component F_n of the tangential force F and binding force F_b are equal [see Figs. 1(b) and 3(b)]. Taking into account obvious expressions for the forces listed in Appendix B, after the elementary calculations presented there, we derive an analytical expression for the minimal length l of the separated graphene region,

$$l = h\sqrt[3]{\frac{Yd}{2J}} > |U|[d_{33} + (1+2\nu)d_{31}]\sqrt[3]{\frac{4Yd}{J}}. \qquad (6)$$

The inequality in Eq. (6) originates from the inequality $h > h_\infty$ (see Fig. 2 with designations). The estimates made from Eq. (6) show that the stretched section can reach tens of nanometers for gate voltages $|U| \geq 3$ V, PZT parameters at room temperature, binding energies $J < 0.25$ J/m^2, and separation $d = 0.5$ nm. For a suspended graphene, the length can be much longer, namely, $l \sim D$ [see magenta curve 2 in Fig. 3(b)].

It is obvious now that the linear approximation of the separated graphene region shown by a dotted line in Fig. 3(b) can be used for the case when the length l of the separated graphene region is at least longer than the half-width $w/2$ of the ferroelectric surface displacement step at the FDW. Substituting the estimate (6) and Eq. (4) at $d \ll H$ in the inequality $l > w/2$, we obtain the condition of the linear approximation validity:

$$|U|\left[d_{33} + (1+2\nu)d_{31}\right]\sqrt[3]{\frac{4Yd}{J}} > \frac{k}{2}H. \qquad (7)$$

For the chosen PZT parameters, the inequality (7) becomes valid, e.g., for relatively thin films ($H < 50$ nm), gate voltages U higher than 3.5 V, binding energies $J < 0.25$ J/m^2, and graphene-ferroelectric separation $d = 0.5$ nm.

Note that thin films (tens of nanometers or thinner) of multiaxial ferroelectric $Pb_xZr_{1-x}TiO_3$ with the composition x near the morphotropic boundary $x = 0.5$ and without perfect electric contact between its surfaces, and electrodes can change their polarization direction from the out-of-plane one to the in-plane one [54,55]. In-plane or closure domains can appear with the film thickness decrease in order to minimize the depolarization field energy in the gap between the graphene layer and ferroelectric surface. For this case, the inequality (7) loses its sense. However, it appears that simple measures can be performed for the validity of Eq. (7). First, the in-plane polarization direction can be more stable than the out-of-plane one in thin PZT film only in the absence of misfit strain or for tensile strains [54,55]. A compressive misfit strain u_m about -0.01 or more can stabilize the out-of-plane polarization in PZT [54–56] and significantly decrease the critical thickness H_{cr} of ferroelectricity disappearance [57] that can be estimated from the formula $H_{cr} \approx \{(H_{DL}+d)/\epsilon_0\epsilon_d[\alpha_T(T-T_C) - 2Q_{12}u_m/(s_{11}+s_{12})]\}$ [58], where $\alpha_T = 2.66\times10^5$ C^{-2}Jm/K, $T_C \approx 666$ K is a ferroelectric Curie temperature, T is the ambient temperature, $Q_{12} \approx -0.0295$ C^{-2} m^4 is the negative electrostriction coefficient, $s_{11} = 8.2\times10^{-12}$ Pa^{-1} and $s_{12} = -2.6\times10^{-12}$ Pa^{-1} are elastic compliances [54,59], ϵ_d is the relative dielectric permittivity of the gap, and $\epsilon_0 = 8.85\times10^{-12}$ F/m is the universal dielectric constant. Because of the orientating role of compressive substrate, the critical thickness of multidomain film can become five lattice constants or even less [60]. Hence, it is enough to deposit the epitaxial PZT film on a mechanically rigid thick compressive substrate like perovskite $SrTiO_3$ [see Fig. 3(b)].

The piezoeffect-induced separated areas of graphene, which are suspended between elongated and shortened domains, can cause many interesting effects, some of which are discussed below.

IV. GRAPHENE CONDUCTANCE

The conductance of the graphene channel in the diffusion regime can change significantly because electrons in the separated stretched section scatter on acoustic phonons [21]. In particular, the voltage dependence of the conductance $G(U)$ of the graphene channel, when its part of length $l(U)$ is separated and another part of length $L - l(U)$ is bounded, obeys the Matiessen rule [21]:

$$G(U) = W\left[\frac{L-\chi|U|}{\sigma_B} + \frac{\chi|U|}{\sigma_S}\right]^{-1}. \quad (8)$$

Here, L is the channel length and W is its width. The separated length $l(U) = \chi|U|$, where the coefficient $\chi = [d_{33} + (1+2\nu)d_{31}]\sqrt[3]{4Yd/J}$ in accordance with Eq. (6). The two addends in the brackets of Eq. (8) correspond to the conductance of the bonded (denoted by subscript "B") and separated (denote by subscript "S") sections of the graphene channel, respectively. Analytical expressions for the conductivities $\sigma_{B,S}$ are derived in Appendix C.

The conductivity of the bounded section has the form

$$\sigma_B = \frac{2e^2}{\pi^{3/2}\hbar}\lambda_B\sqrt{n_S}. \quad (9)$$

Here, $e = 1.6\times10^{-19}$ C is elementary charge, $\hbar = 1.056\times10^{-34}$ J s $= 6.583\times10^{-16}$ eV s is the Plank constant, $v_F = 10^6$ m/s is characteristic electron velocity in graphene, and λ_B is the mean free path in the graphene channel. The concentration of 2D electrons n_S can be regarded as a constant voltage-independent value far from the FDWs, namely, $n_S \approx |P_S/e|$ (see Appendix C). Using that for the most common case of electron scattering in graphene channel at ionized impurities in a substrate $\lambda_B[n_S] = \alpha\sqrt{n_S}$, where the proportionality coefficient α depends on the substrate material and graphene-ferroelectric interface chemistry [see Eqs. (3.20)–(3.22) in Ref. [3] and Appendix D], we obtain from Eq. (9) the dependence $\sigma_B[n_S]=[(2e^2\alpha)/(\pi^{3/2}\hbar)]n_S\approx8.75\times10^{-5}\alpha n_S$ (in Siemens). Taking into account that the P_S value can be 10 times smaller for thin films than its bulk value, the concentration varies in the range $n_S \cong (0.3\text{–}3)\times10^{18}$ m^{-2} depending on the film thickness but should be regarded as a voltage- and coordinate-independent constant far from the FDW. Thus, elementary estimates give $\sigma_B \cong (0.15-15)\times10^{-3}$ Ω^{-1} for reasonable ranges of λ_B=10–100nm and $P_S = 0.05\text{–}0.5$ C/m^2.

On the contrary, the main channel for electron scattering in the separated stretched section of structurally perfect graphene is collisions with acoustic phonons. In this case, $\lambda_S(E) \sim 1/E$ [21]. This leads to a paradoxical, however, well-known result. Conductivity σ_S does not depend on 2D electron concentration in the graphene channel. Hence, for further estimations, we use a well-known upper limit for σ_S [3]:

$$\sigma_S = \frac{4e^2\hbar\rho_m v_F^2 v_S^2}{\pi D_A^2 k_B T}. \quad (10)$$

Here, $\rho_m \approx 7.6\times10^{-7}$ kg/m^2 is the 2D mass density of carriers in graphene, $v_S \approx 2.1\times10^4$ m/s is a sound velocity in graphene, Boltzmann constant $k_B = 1.38\times10^{-23}$ J/K,

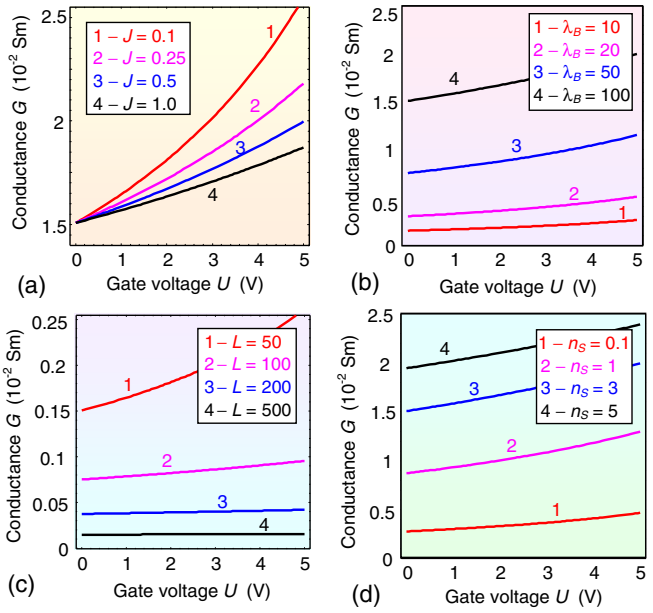

FIG. 4 Dependences of the conductance $G(U)$ on the gate voltage U calculated for several values (curves 1–4) of binding energy $J = 0.1, 0.25, 0.5, 1.0$ J/m^2 (a); electron mean free path $\lambda_B = 10, 20, 50, 100$ nm (b); channel length $L = 50, 100, 200, 500$ nm (c); concentration $n_S = (0.1, 1, 3, 5)\times10^{18}$ m^{-2} (d). Piezoelectric coefficients $d_{33} \approx 10^3$ pm/V, $d_{31} \approx -450$ pm/V, and Poisson ratio $v = 0.3$ corresponds to $PbZr_{0.5}Ti_{0.5}O_3$, $n_S = 3\times10^{18}$ m^{-2}, $\lambda_B = 100$ nm, $L = 50$ nm, $W = 50$ nm, and separation $d = 0.5$ nm, graphene Young's modulus $Y = 1$ TPa, and binding energy $J = 0.5$ J/m^2.

and $D_A \approx 19$ eV is the acoustic deformation potential that describes electron-phonon interaction. Expression (10) yields $\sigma_S \approx 3.4\times10^{-2}$ Ω^{-1} at room temperature.

Figures 4–6 present the conductance G calculated from Eqs. (8)–(10) for different values of gate voltage U, electron mean free path in graphene λ_B, electron concentration n_S, binding energy J, graphene-ferroelectric separation d, and channel length L. The conductance in Eq. (8) is linearly proportional to the channel width W that is chosen equal to 50 nm. Parameters $d_{33} \approx 10^3$ pm/V, $d_{31} \approx -450$ pm/V, and the Poisson ratio $v = 0.3$ corresponds to PZT. The graphene Young's modulus is $Y = 1$ TPa and conductance $\sigma_S = 3.4\times10^{-2}$ Ω^{-1}. Other parameters vary within physically reasonable intervals, namely, concentration 0.1×10^{18} m$^{-2} \le n_S \le 5\times10^{18}$ m^{-2}, binding energies 0.1 J/m$^2 \le J \le 1$ J/m^2, electron mean free path 10 nm $\le \lambda_B \le 100$ nm, channel length 50 nm $\le L \le 500$ nm, and separation 0.1 nm $\le d \le 1$ nm. The behavior illustrated by Figs. 4–6 can be qualitatively explained by approximate expression (C5) for the inverse conductance derived in Appendix C.

The conductance increases with the U increase; and the increase is monotonic and faster than linear (i.e., "super-linear") at other fixed parameters (Fig. 4). The increase is

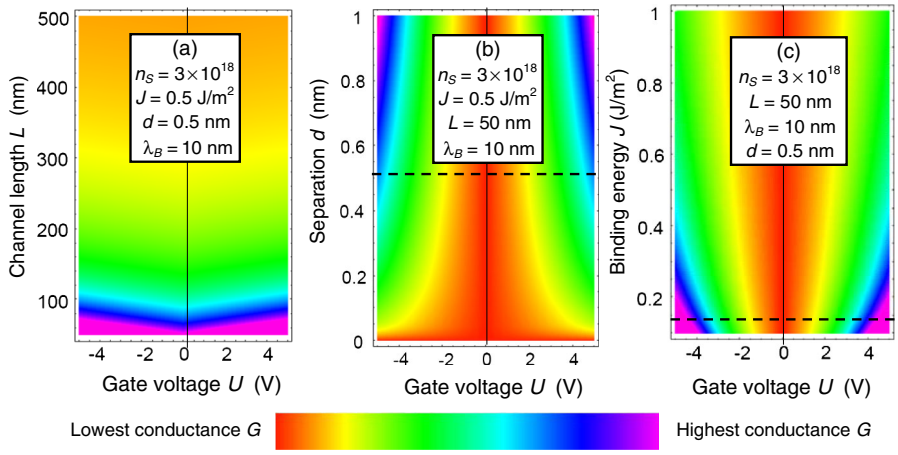

FIG. 5 Contour maps of the conductance $G(U)$ in different coordinates $\{U, L\}$ (a), $\{U, d\}$ (b), and $\{U, J\}$ (c). Fixed parameters are listed in the legends. Other parameters are the same as in Fig. 4. Color scale ranges from 0.015 Sm (red) to 0.262 Sm (violet) for map (a); from 0.151 Sm (red) to 0.324 Sm (violet) for map (b); from 0.151 Sm (red) to 0.550 Sm (violet) for map (c).

the most pronounced at small binding energies $J \leq 0.2$ J/m^2 [Fig. 4(a)], long mean free paths $\lambda_B \geq 50$ nm [Fig. 4(b)], small channel length $L \leq 100$ nm [Fig. 4(c)], and relatively high concentrations $n_S \geq 10^{18}$ m^{-2} [Fig. 4(d)].

As one can see from Fig. 4, the conductance ratio $G(U)/G(0)$ does not exceed 1.25 for the case of graphene partial separation [presented by the red curve in Fig. 3(b)] at realistic values of parameters. However, it can be significantly greater if the domain stripe period D is much shorter than the channel length L. For this case, length L is divided into two almost equal parts between the separated and bonded sections (i.e., $l \approx L/2$). If the p-n junctions at the FDW do not change the general conductance of the graphene channel significantly [2] and the electron mean free pass $\lambda_{B.S} \ll D$ and $\sigma_S \gg \sigma_B$, Eq. (8) yields $\{[G(U)]/[G(0)]\} = \{1 - [1 - (\sigma_B/\sigma_S)][l(U)/L]\}^{-1} \approx 2$. Thus, the experimental situation [2] leads to a rather high conductance ratio. Note that the ratio $G(U)/G(0)$ can be significantly greater than 2, e.g., in the case of mostly suspended graphene ($l \approx L$) with $\sigma_S \gg \sigma_B$. However, the possibility of such a limiting case needs special examination.

Actually, the possibility $G(U)/G(0) \gg 1$ follows from Figs. 5(a)–5(c), which are colored contour maps of the conductance dependence on coordinate pairs such as $\{U, L\}$, $\{U, d\}$, and $\{U, J\}$. The horizontal lines in Figs. 5(b) and 5(c) show the pronounced charges of $G(U)$ (from 0.15 to 0.55 Sm) with U increase from 0 to 5 V. It appears that the conductance linearly increases with the ratio $|U|/L$ increase [see the V-type colored contours in Fig. 5(a)]. The conductance dependences on the parameters d, J, and $|U|$ are, in fact, the dependence on the ratio $2|U|\sqrt[3]{Yd/2J}$ when its value becomes significant [compare the colored contours in Figs. 5(b) and 5(c)].

As seen from the color scale in Figs. 5(b) and 5(c), the pronounced changes of $G(U)$ (about 2.1–3.6 times) in comparison with its reference value $G(0) = W\sigma_B/L$ correspond to relatively high concentrations $n_S \geq 10^{18}$ m^{-2}, small binding energy $J \leq 0.2$ J/m^2, realistic separation $d = 0.5$ nm, and small channel length $L \leq 100$ nm. Small binding energy makes the partial separation or complete exfoliation of graphene easier and the separated areas longer. Small channel length means the quasiballistic regime of current in the bonded graphene channel section. In the opposite case of a diffusive regime, the total conductance is too low and cannot be changed significantly by a suspended section.

At fixed gate voltage (3 V), the conductance strongly decreases with an L increase from 50 to 500 nm, and the changes in 1–2 orders of magnitude correspond to small $\lambda_B \leq 50$ nm [Fig. 6(a)]. In fact, we can interpret Fig. 6(a) as

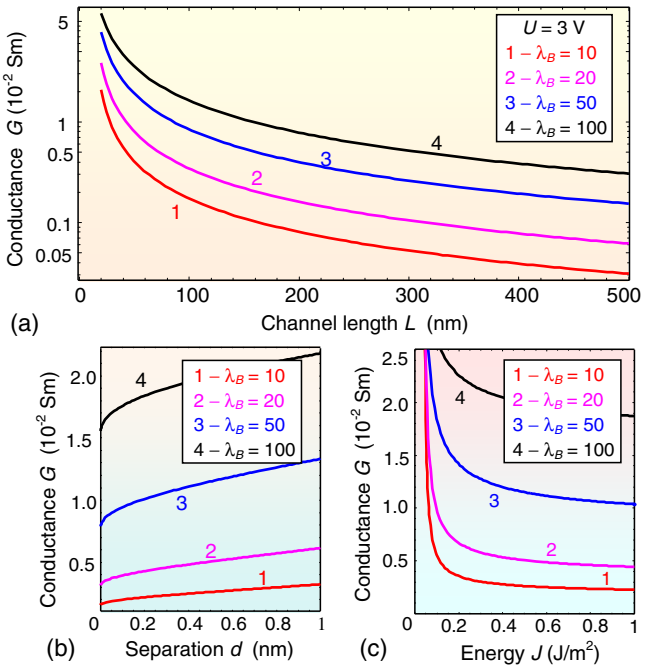

FIG. 6 (a) Dependences of the conductance $G(U)$ on the channel length L calculated for gate voltage $U = 3$ V and several values of electron mean free path $\lambda_B = 10$, 20, 50, 100 nm (curves 1–4). (b),(c) Conductance $G(U)$ dependence on the separation d (c) and binding energy J (d). Other parameters are the same as in Fig. 4.

a demonstration of the extrinsic size effect of the conductance ("L-size effect"). Conductance dependence on the separation d is a monotonically increasing one but rather weak at $d > 0.2$ nm [Fig. 6(b)], while its dependence on L and λ_B is much more pronounced [compare to Fig. 6(a)]. Conductance dependence on J is a monotonically decreasing one and also rather weak at $J > 0.2$ J/m^2 [Fig. 6(c)].

The prediction of high ratios $G(U)/G(0)$ [see Figs. 5(b) and 5(c)] and its size effects [see Fig. 6(a)] is promising for advanced applications. Several possibilities are discussed in the next section.

V. DISCUSSION OF POTENTIAL APPLICATIONS

Our calculations predict that the piezoelectric effect in the ferroelectric $PbZr_xTi_{1-x}O_3$ ($x \approx 0.5$) leads to its surface displacement about 0.5–1 nm for the gate voltage 2–4 V and room temperature. The displacement can lead to the graphene separation from the substrate, since the density of the graphene-ferroelectric binding energy is relatively small, and the Young's modulus of graphene is extremely high. The length of the separated section is estimated within a simple analytical model showing that it can be 10-nm order or even longer. The separated sections of the graphene channel induced by the piezoeffect can cause interesting physical effects, which are interesting for fundamental physics. First, the conductance of the graphene channel in the diffusion regime changes significantly because the electrons in the stretched section scatter on acoustic phonons [21]. Second, mechanic vibrations of megahertz range can be realized here [61]. Third, high pseudomagnetic fields were reported for stretched graphene [62].

The consideration of the first of these three effects, performed in this work, are promising for advanced applications of graphene on ferroelectric with domain structure in GFETs and related memory elements, various logic devices, as well as for design of highly efficient hybrid electrical modulators, rectifiers, and transducers of voltage-to-current type [7–16,21].

The above-mentioned applications use the fact that the concentration of 2D electrons in the graphene channel on PZT substrate is extremely high (approximately 10^{18} m^{-2}). This value is at least 1–2 orders higher than the maximal values obtained for graphene on ordinary mica substrate (see, e.g., Ref. [63]). For dielectric substrate, concentrations higher than 10^{17} m^{-2} cannot be realized because of the electric breakdown in the substrate appearing under the gate-voltage increase. Therefore, the conductance of graphene on PZT substrate is 1 or 2 orders higher than for the case of a dielectric substrate. Also, it linearly depends on 2D carrier concentration for the common case of dominant scattering at surface-ionized impurities. However, as we demonstrate above, the conductance strongly and nonlinearly depends on the gate voltage at small binding energies [see Figs. 5(b) and 5(c)] and channel length [see Fig. 6(a)].

The steep dependence $G(U)/G(0)$ induced by the piezoeffect in GFET can lead to the noticeable increase (from 1.5 to 3.5 times) of the voltage-to-current conversion coefficient in hybrid electrical modulators, which contain graphene on ferroelectric with FDWs. An essential advantage of the graphene conductance modulation by the piezoeffect at FDWs proposed in this work in comparison with our earlier studies (see Ref. [16] and references therein) is the following. The ferroelectric domains remain immobile in the horizontal direction x, and relatively low gate voltage [64] creates almost instantly [65] the vertical z-displacement steps across the FDWs due to the piezoelectric effect [see Figs. 7(a)–7(c)]. Since the dependence $G(U)$ is voltage symmetric, $G(U) = G(-U)$, the voltage-to-current conversion takes place at double frequency.

In contrast, the controllable motion of FDWs is required in the horizontal x direction along the channel for the noticeable changes of graphene conductance and electroresistance without taking the piezoelectric effect into consideration [16]. The FDW's motion is sluggish and has a voltage threshold; i.e., it requires gate voltages higher that the coercive voltage of polarization reversal. As a matter of fact, it is much easier to create immobile FDWs, which are fixed spontaneously by existing pinning centers and lattice barriers, than to control the inertial motion of FDWs in the presence of unavoidable pinning centers [46]. Hence, the electrical transducers, modulators, and logic memory elements based on graphene on ferroelectric with FDWs, which operate using the piezoelectric displacement

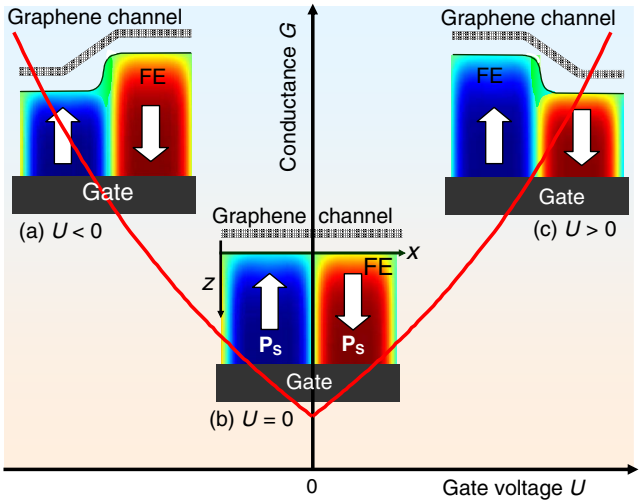

FIG. 7 Modulation of graphene channel conductance by the piezoeffect in GFET on ferroelectric (FE) substrate. The main plot shows the schematic dependence of the channel conductance $G(U)$ on the gate voltage U. Insets (a) and (c) illustrate the vertical piezoelectric displacement of ferroelectric surface at FDW that causes partial separation of graphene sections induced by negative and positive gate voltages, respectively. The displacement and corresponding graphene separation are absent at $U = 0$ [inset (b)].

of immobile ferroelectric domain structure, can be significantly more efficient, much faster, and better controllable than their analogs requiring the motion of FDWs. One can assume that due to the absence of the moving walls, the durability of such modulators can be significantly longer. However, the possibility of graphene complete exfoliation (instead of controllable partial separation) should be foreseen, estimated, and excluded for real applications. Based on our theoretical estimates, this exfoliation can be realized by choosing an optimal material of the ferroelectric substrate and its thickness. The most serious challenge in the applications is how to control the graphene-ferroelectric binding energy and separation.

The joint action of the piezoelectric and finite size effects should have a pronounced impact on the nonlinear hysteretic dynamics of the FDWs, stored charge, and electroresistance in the graphene-on-ferroelectric nanostructures with p-n junction potentials [16,44]. This impact allows advanced applications of the nanostructures as ultrasensitive piezoresistive elements. The idea of such an element is to deposit the graphene cover on the surface of ferroelectric film with high piezoelectric response. Because of the strong dependence of graphene conductance and electroresistance on the piezoelectric displacement of a ferroelectric surface, its electrical response to applied voltage and/or electromechanical efficiency can increase several times. The increase depends on the ferroelectric domain structure and FDW amount, ferroelectric film thickness and its piezoelectric coefficients, graphene-ferroelectric separation, and binding energy.

The obtained results also have implications for applications of a graphene sheet stretched by FDW in mechanical resonators and pseudomagnetic field generators, and the applications could be a subject of further studies.

Finally, we underline that since graphene discovery and up to now the suspended areas in graphene channel were fabricated over trenches in the substrate (see, e.g., Ref. [61]). Here we propose an alternative method of suspended areas fabrication based on the piezoeffect in a ferroelectric substrate. The method does not require any additional technological procedures like chemical etching or mechanical treating of the substrate surface. It can be used, among other things, to fabricate electromechanical nanosystems for the sensing of single molecules and even electrons (as proposed in Ref. [61]).

VI. CONCLUSIONS

To conclude, p-n junctions in graphene on FDWs have been actively studied recently, but the role of the piezoelectric effect in a ferroelectric substrate was not considered. We propose a piezoelectric mechanism of conductance control in the GFET on a ferroelectric substrate with immobile domain walls. In particular, we predict that the graphene channel conductance can be controlled by the gate voltage due to the piezoelectric elongation and contraction of ferroelectric domains with opposite polarization directions. At the same time, the gate voltage does not change significantly the 2D carrier concentration in graphene. However, it can create the bonded, separated, suspended, and stretched sections of the graphene sheet, whose conductivity and resistivity are significantly different. Our calculations demonstrate the possibility of a several times increase of GFET conductance for ferroelectric substrates with high piezoelectric response.

Taking into account that the conductance of the graphene on a ferroelectric is significantly higher than the one of graphene on ordinary dielectric substrates, the predicted effect can be very useful for improvement and miniaturization of various electronic devices (such as advanced logic elements, memory cells, highly efficient hybrid electrical modulators and voltage-to-current transducers with frequency doubling and relatively low operation voltages, and piezoresistive elements).

Also, we propose an alternative method of suspended graphene areas fabrication based on the piezoeffect in a ferroelectric substrate. The method does not require any additional technological procedures like chemical etching or mechanical treating of the substrate surface.

ACKNOWLEDGMENTS

Authors express their deep gratitude to the referees for useful suggestions and help with the manuscript's improvement. This paper contains the results of studies conducted by the President of Ukraine grant for competitive projects (Grant No. F74/25879) of the State Fund for Fundamental Research (A. I. K. and A. N. M.). A portion of this research is conducted at the Center for Nanophase Materials Sciences, which is a Department of Energy Office of Science User Facility, Project No. CNMS2016-061.

APPENDIX A: SURFACE DISPLACEMENT FOR PERFECT CONTACT

In the particular case of a perfect contact ($d = 0$), Eqs. (1)–(3) for the surface displacement simplify to

$$u_3(x, d \to 0) = -\frac{2U}{\pi}\left\{\left[d_{33} + (1+2v)d_{31}\right]\arctan\left(\frac{x}{H}\right) + (d_{33} + v d_{31})\frac{x}{H}\ln\left(1+\frac{H^2}{x^2}\right)\right\}. \quad \text{(A1)}$$

APPENDIX B: ELASTIC FORCES CALCULATIONS

It is natural to expect that the graphene separation occurs right to the point, where the normal component F_n of the elastic tension force F and binding force F_b are equal [see Figs. 1(b) and 3(b)]. Namely,

$$|F_n| = |F_b|. \tag{B1}$$

Taking into account the obvious expressions for the forces shown in Fig. 1(b),

$$|F| = \frac{YS\Delta l}{l}, \qquad |F_n| = \frac{YS\Delta l}{l}\sin\alpha,$$
$$|F_S| = \frac{YS\Delta l}{l}\cos\alpha \approx \frac{YS\Delta l}{l}, \qquad |F_b| \approx \frac{JS}{d}, \tag{B2}$$

where S is the effective cross section of the carbon atom in graphene, and l is the length of the separated graphene region. Because of the strong inequality $l \gg \Delta l$, we obtain that $h^2 + l^2 = (l + \Delta l)^2 \approx l^2 + 2l\Delta l$ and so $\Delta l = h^2/2l$. Substituting the approximations $\Delta l = h^2/2l$ and $\sin\alpha \approx \alpha \approx h/l$ in the expressions (B2), we obtain the normal force $|F_n| \approx [(YSh^3)/l^3]$. Then, substituting the expression (5) for $h_\infty < h$ in the equality (B1), we finally get

$$l = h\sqrt[3]{\frac{Yd}{2J}} > 2|U|[d_{33} + (1 + 2\nu)d_{31}]\sqrt[3]{\frac{Yd}{2J}}. \tag{B3}$$

The inequality in Eq. (B3) originates from the inequality $h > h_\infty$.

APPENDIX C: CONDUCTANCE CALCULATIONS

The conductance G of graphene channel with length L and width W, when some part of the channel with length $l(U)$ is suspended, can be presented according to the Matiessen rule [21] as

$$\frac{1}{G(U)} = \frac{1}{W}\left[\frac{L - l(U)}{\sigma_B} + \frac{l(U)}{\sigma_S}\right]. \tag{C1}$$

The conductivities $\sigma_{B,S}$ can be presented as [21]

$$\sigma_{B,S} = \frac{e^2}{\pi\hbar}\left(\frac{2E_F}{\pi\hbar v_F}\right)\lambda_{B,S}(E_F). \tag{C2}$$

Here, $e = 1.6 \times 10^{-19}$ C is the elementary charge, $\hbar = 1.056 \times 10^{-34}$ J s $= 6.583 \times 10^{-16}$ eV s is the Plank constant, $E_F \cong \hbar v_F\sqrt{\pi n_S(U, P_S)}$ is the Fermi energy in graphene, $v_F = 10^6$ m/s is the characteristic electron velocity in graphene, and $\lambda_{B,S}(E_F)$ is the electron mean free path in bonded and separated sections of the graphene channel, respectively.

The dominant mechanism for electron scattering in graphene on substrate is scattering by ionized impurities in the substrate. In this case, the electron mean free path $\lambda_B(E) \sim E$ [3]. Allowing for the well-known relation $n_S(E_F) = [E_F^2/(\pi\hbar^2 v_F^2)]$, one is led to the following dependence of conductivity (C2) on 2D electrons concentration n_S and mean free path λ_B in the graphene channel,

$$\sigma_B = \frac{2e^2}{\pi^{3/2}\hbar}\lambda_B\sqrt{n_S} \approx 8.75 \times 10^{-5}\lambda_B\sqrt{n_S} \quad \text{(in Siemens)}. \tag{C3}$$

The expression (C3) should account for the dependence of n_S on the ferroelectric polarization $P_S(x)$ and gate voltage U. The expressions used in Refs. [3,66] show that the carrier density is proportional to the difference of the electric displacement normal components, $D_z(x, 0) - D_z(x, -d)$, i.e., $en_S(x) \cong P_S(x) + \epsilon_0\epsilon_b E_z(x)$, where $\epsilon_0 = 8.85 \times 10^{-12}$ F/m is a universal dielectric constant, and $\epsilon_b \cong 5$ is a background permittivity of PZT [67] that is much smaller than the static ferroelectric permittivity $\epsilon_f \sim 500$. The small value of the background permittivity is conditioned by the fact that it is unrelated with the soft-mode contributions and contains contributions from other modes as well as electronic contribution.

Since the spontaneous polarization saturates far from the FDW [$P_S(x) \to \pm P_S$], the concentration is

$$n_S \sim |\pm\frac{P_S}{e} + \frac{\epsilon_0\epsilon_b U}{e(H + d)}|. \tag{C4}$$

At gate voltage $U = 1$ V, film thickness $H = 50$ nm, and separation $d = 0.5$ nm, the second contribution to the concentration in Eq. (C4) $[(\epsilon_0\epsilon_b U)/(H + d)] \cong 0.001$ C/m^2 is much smaller than the first one P_S/e for $P_S = 0.5$ C/m^2 corresponding to bulk PZT at room temperature.

The behavior illustrated by Figs. 4–6 can be explained by analytical expression (C1) for the inverse conductance, where the length l of the separated section is proportional to the ratio $l \sim |U|\sqrt[3]{Yd/2J}$ and the conductivity $\sigma_B \sim \lambda_B\sqrt{n_S} \sim n_S \sim \lambda_B^2$ according to Eq. (C3). Thus, the inverse conductance has two contributions from the bonded and separated sections, $\{1/[G_B(U)]\} \sim [1/(\lambda_B\sqrt{n_S})]\{L - 2[d_{33} + (1 + 2\nu)d_{31}]\sqrt[3]{(Yd)/(2J)}|U|\}$ and $\{1/[G_S(U)]\} \sim \sqrt[3]{(Yd)/(2J)}(|U|/\sigma_S)$, respectively. Since the inequalities $\sigma_S > \sigma_B$ or $\sigma_S \gg \sigma_B$ are valid in accordance with our estimates, the first contribution dominates if the strong inequality $l \ll L$ is valid, and so

$$G(U) \sim \frac{\lambda_B\sqrt{n_S}}{L - 2|U|[d_{33} + (1 + 2\nu)d_{31}]\sqrt[3]{Yd/2J}}. \tag{C5}$$

APPENDIX D: RELAXATION TIME CALCULATIONS

Using Eqs. (3.20)–(3.22) from Ref. [3], one gets the expression for the relaxation time

$$\tau = \frac{\tau_0}{G[2r_s]} = \frac{\sqrt{n_s}}{2\sqrt{\pi}n_{\text{imp}}v_F G[2r_s]}, \tag{D1}$$

$$\frac{G[x]}{x} = \frac{\pi}{4} + 3x - \frac{3\pi x^2}{2} + \frac{x(3x^2 - 2)\arccos[1/x]}{\sqrt{x^2 - 1}}. \tag{D2}$$

Here, r_s is the interaction parameter (coupling constant), the values $r_s = 2.19/\epsilon_b$ and $\epsilon_b = 5$ is a background dielectric constant. The mean free path is given by the expression

$$\lambda_B = \frac{\pi}{2}\tau v_F = \frac{\pi}{2} v_F \frac{\sqrt{n_s}}{2\sqrt{\pi} n_{\mathrm{imp}} v_F} \frac{1}{G[2r_s]} = \frac{\sqrt{\pi n_s}}{4 n_{\mathrm{imp}} G[2r_s]} = \alpha\sqrt{n_s}. \quad \text{(D3)}$$

For the coefficient α, we finally get

$$\alpha = \frac{\sqrt{\pi}}{4 n_{\mathrm{imp}} G[2r_s]}\,[m^2], \quad \text{(D4)}$$

where $G[2r_s]$ is a function of the coupling constant, and n_{imp} is the impurity concentration.

[1] K. Novoselov, A. Geim, S. Morozov, D. Jiang, Y. Zhang, S. Dubonos, I. Grigorieva, and A. Firsov, Electric field effect in atomically thin carbon films, Science **306**, 666 (2004).

[2] A. Geim, Graphene: Status and prospects, Science **324**, 1530 (2009).

[3] S. Das Sarma, Shaffique Adam, E. H. Hwang, and E. Rossi, Electronic transport in two-dimensional graphene, Rev. Mod. Phys. **83**, 407 (2011).

[4] B. Amorim, A. Cortijo, F. de Juan, A. G. Grushin, F. Guinea, A. Gutierrez-Rubio, H. Ochoa, V. Parente, R. Roldan, P. San-Jose, J. Schiefele, M. Sturla, and M. A. H. Vozmediano, Novel effects of strains in graphene and other two dimensional materials, Phys. Rep. **617**, 1 (2016).

[5] Gerardo G. Naumis, Salvador Barraza-Lopez, Maurice Oliva-Leyva, and Humberto Terrones, A review of the electronic and optical properties of strained graphene and other similar 2D materials, Rep. Prog. Phys. **80**, 096501 (2017).

[6] Zhiyong Xiao, Jingfeng Song, David K. Ferry, Stephen Ducharme, and Xia Hong, Ferroelectric-Domain-Patterning-Controlled Schottky Junction State in Monolayer MoS_2, Phys. Rev. Lett. **118**, 236801 (2017).

[7] Yi Zheng, Guang-Xin Ni, Chee-Tat Toh, Chin-Yaw Tan, Kui Yao, and Barbaros Özyilmaz, Graphene Field-Effect Transistors with Ferroelectric Gating, Phys. Rev. Lett. **105**, 166602 (2010).

[8] Woo Young Kim, Hyeon-Don Kim, Teun-Teun Kim, Hyun-Sung Park, Kanghee Lee, Hyun Joo Choi, Seung Hoon Lee, Jaehyeon Son, Namkyoo Park, and Bumki Min, Graphene-ferroelectric metadevices for nonvolatile memory and reconfigurable logic-gate operations, Nat. Commun. **7**, 10429 (2016).

[9] X. Hong, J. Hoffman, A. Posadas, K. Zou, C. H. Ahn, and J. Zhu, Unusual resistance hysteresis in n-layer graphene field effect transistors fabricated on ferroelectric $Pb(Zr_{0.2}Ti_{0.8})O_3$, Appl. Phys. Lett. **97**, 033114 (2010).

[10] A. Rajapitamahuni, J. Hoffman, C. H. Ahn, and X. Hong, Examining graphene field effect sensors for ferroelectric thin film studies, Nano Lett. **13**, 4374 (2013).

[11] M. Humed Yusuf, B. Nielsen, M. Dawber, and X. Du, Extrinsic and intrinsic charge trapping at the graphene/ferroelectric interface, Nano Lett. **14**, 5437 (2014).

[12] J. H. Hinnefeld, Ruijuan Xu, S. Rogers, Shishir Pandya, Moonsub Shim, L. W. Martin, and N. Mason, Single gate PN junctions in graphene-ferroelectric devices, arXiv:1506.07138.

[13] C. Baeumer, D. Saldana-Greco, J. M. P. Martirez, A. M. Rappe, M. Shim, and L. W. Martin, Ferroelectrically driven spatial carrier density modulation in graphene, Nat. Commun. **6**, 6136 (2015).

[14] Anna N. Morozovska, Eugene A. Eliseev, and Maksym V. Strikha, Ballistic conductivity of graphene channel with p-n junction on ferroelectric domain wall, Appl. Phys. Lett. **108**, 232902 (2016).

[15] Maksym V. Strikha and Anna N. Morozovska, Limits for the graphene on ferroelectric domain wall p-n-junction rectifier for different regimes of current, J. Appl. Phys. **120**, 214101 (2016).

[16] Anatolii I. Kurchak, Eugene A. Eliseev, Sergei V. Kalinin, Maksym V. Strikha, and Anna N. Morozovska, p-n Junction Dynamics Induced in a Graphene Channel by Ferroelectric-Domain Motion in the Substrate, Phys. Rev. Applied **8**, 024027 (2017).

[17] J. R. Williams, L. DiCarlo, and C. M. Marcus, Quantum Hall effect in a gate-controlled pn junction of graphene, Science **317**, 638 (2007).

[18] V. V. Cheianov and V. I. Falko, Selective transmission of Dirac electrons and ballistic magnetoresistance of n-p junctions in graphene, Phys. Rev. B **74**, 041403 (2006).

[19] J. R. Whyte and J. M. Gregg, A diode for ferroelectric domain-wall motion, Nat. Commun. **6**, 7361 (2015).

[20] L. M. Zhang and M. M. Fogler, Nonlinear Screening and Ballistic Transport in a Graphene p-n Junction, Phys. Rev. Lett. **100**, 116804 (2008).

[21] Yu. A. Kruglyak and M. V. Strikha, Generalized Landauer-Datta-Lundstrom model in application to transport phenomena in graphene, Ukr. J. Phys. Rev. **10**, 3 (2015).

[22] C. W. Beenakker, Andreev reflection and Klein tunneling in graphene, Rev. Mod. Phys. **80**, 1337 (2008).

[23] M. I. Katsnelson, K. S. Novoselov, and A. K. Geim, Chiral tunnelling and the Klein paradox in graphene, Nat. Phys. **2**, 620 (2006).

[24] V. V. Cheianov, V. I. Falko, and B. L. Altshuler, The focusing of electron flow and a Veselago lens in graphene p-n junctions, Science **315**, 1252 (2007).

[25] A. N. Morozovska and M. V. Strikha, Pyroelectric origin of the carrier density modulation at graphene-ferroelectric interface, J. Appl. Phys. **114**, 014101 (2013).

[26] A. N. Morozovska, E. A. Eliseev, A. V. Ievlev, O. V. Varenyk, A. S. Pusenkova, Ying-Hao Chu, V. Ya. Shur, M. V. Strikha, and S. V. Kalinin, Ferroelectric domain triggers the charge modulation in semiconductors, J. Appl. Phys. **116**, 066817 (2014).

[27] I. I. Naumov and A. M. Bratkovsky, Gap opening in graphene by simple periodic inhomogeneous strain, Phys. Rev. B **84**, 245444 (2011).

[28] T. L. Linnik, Effective Hamiltonian of strained graphene, J. Phys. Condens. Matter **24**, 205302 (2012).

[29] T. L. Linnik, Photoinduced valley currents in strained graphene, Phys. Rev. B **90**, 075406 (2014).

[30] M. J. Haun, E. Furman, S. J. Jang, and L. E. Cross, Thermodynamic theory of the lead zirconate-titanate solid solution system, Part V: Theoretical calculations, Ferroelectrics **99**, 63 (1989) (see Fig. 16 and Table I).

[31] Steven P. Koenig, Narasimha G. Boddeti, Martin L. Dunn, and J. Scott Bunch, Ultrastrong adhesion of graphene membranes, Nat. Nanotechnol. **6**, 543 (2011).

[32] Antonio Politano and Gennaro Chiarello, Probing the Young's modulus, and Poisson's ratio in graphene/metal interfaces, and graphite: A comparative study, Nano Res. **8**, 1847 (2015).

[33] Tao Chen and Rebecca Cheung, *Graphene Science Handbook. Mechanical and Chemical Properties* (CRC Press, Boca Raton, 2016), pp. 3–15.

[34] S. V. Kalinin, B. J. Rodriguez, S.-H. Kim, S.-K. Hong, A. Gruverman, and E. A. Eliseev, Imaging mechanism of piezoresponse force microscopy in capacitor structures, Appl. Phys. Lett. **92**, 152906 (2008).

[35] F. Felten, G. A. Schneider, J. Muñoz Saldaña, and S. V. Kalinin, Modeling and measurement of surface displacements in $BaTiO_3$ bulk material in piezoresponse force microscopy, J. Appl. Phys. **96**, 563 (2004).

[36] S. V. Kalinin, E. A. Eliseev, and A. N. Morozovska, Materials contrast in piezoresponse force microscopy, Appl. Phys. Lett. **88**, 232904 (2006).

[37] A. N. Morozovska, E. A. Eliseev, S. L. Bravina, and S. V. Kalinin, Resolution function theory in piezoresponse force microscopy: Domain wall profile, spatial resolution, and tip calibration, Phys. Rev. B **75**, 174109 (2007).

[38] S. V. Kalinin, A. N. Morozovska, L. Q. Chen, and B. J. Rodriguez, Local polarization dynamics in ferroelectric materials, Rep. Prog. Phys. **73**, 056502 (2010).

[39] Note that $v = -s_{12}/s_{11}$, where s_{ij} are elastic compliances.

[40] A. M. Bratkovsky and A. P. Levanyuk, Effects of anisotropic elasticity in the problem of domain formation and stability of monodomain state in ferroelectric films, Phys. Rev. B **84**, 045401 (2011).

[41] E. V. Chensky and V. V. Tarasenko, Theory of phase transitions to inhomogeneous states in finite ferroelectrics in an external electric field, Zh. Eksp. Teor. Fiz. **83**, 1089 (1982) [Sov. Phys. JETP **56**, 618 (1982)].

[42] A. K. Tagantsev, L. E. Cross, and J. Fousek, *Domains in Ferroic Crystals and Thin Films* (Springer, New York, 2010), ISBN 978-1-4419-1416-3, e-ISBN 978-1-4419-1417-0.

[43] Ivan S. Vorotiahin, Eugene A. Eliseev, Qian Li, Sergei V. Kalinin, Yuri A. Genenko, and Anna N. Morozovska, Tuning the polar states of ferroelectric films via surface charges and flexoelectricity, Acta Mater. **137**, 85 (2017).

[44] A. N. Morozovska, A. S. Pusenkova, O. V. Varenyk, S. V. Kalinin, E. A. Eliseev, and M. V. Strikha, Finite size effects of hysteretic dynamics in multi-layer graphene on ferroelectric, Phys. Rev. B **91**, 235312 (2015).

[45] A. S. Sidorkin, *Domain Structure in Ferroelectrics and Related Materials* (Cambridge International Science Publishing, Cambridge, England, 2006).

[46] A. K. Tagantsev, L. E. Cross, and J. Fousek, *Domains in Ferroic Crystals and Thin Films* (Springer, New York, 2010), ISBN 978-1-4419-1416-3, e-ISBN 978-1-4419-1417-0.

[47] E. A. Eliseev, S. V. Kalinin, and A. N. Morozovska, Finite size effects in ferroelectric-semiconductor thin films under open-circuit electric boundary conditions, J. Appl. Phys. **117**, 034102 (2015).

[48] A. M. Bratkovsky and A. P. Levanyuk, Continuous theory of ferroelectric states in ultrathin films with real electrodes, J. Comput. Theor. Nanosci. **6**, 465 (2009).

[49] T. Mitsui and J. Furuichi, Domain structure of Rochelle salt and KH_2PO_4, Phys. Rev. **90**, 193 (1953).

[50] T. J. Yang, V. Gopalan, P. J. Swart, and U. Mohideen, Direct Observation of Pinning and Bowing of a Single Ferroelectric Domain Wall, Phys. Rev. Lett. **82**, 4106 (1999).

[51] S. Choudhury, Y. Li, N. Odagawa, Aravind Vasudevarao, L. Tian, P. Capek, V. Dierolf, A. N. Morozovska, E. A. Eliseev, S. V. Kalinin, Y. Cho, L.-Q. Chen, and V. Gopalan, The influence of 180° ferroelectric domain wall width on the threshold field for wall motion, J. Appl. Phys. **104**, 084107 (2008).

[52] Rakesh K. Behera, Chan-Woo Lee, Donghwa Lee, Anna N. Morozovska, Susan B. Sinnott, Aravind Asthagiri, Venkatraman Gopalan, and Simon R. Phillpot, Structure and energetics of 180° domain walls in $PbTiO_3$ by density functional theory, J. Phys. Condens. Matter **23**, 175902 (2011).

[53] Leo J. McGilly, Ludwig Feigl, and Nava Setter, Dynamics of ferroelectric 180° domain walls at engineered pinning centers, Appl. Phys. Lett. **111**, 022901 (2017).

[54] N. A. Pertsev, V. G. Kukhar, H. Kohlstedt, and R. Waser, Phase diagrams and physical properties of single-domain epitaxial $Pb(Zr_{1-x}Ti_x)O^3$ thin films, Phys. Rev. B, **67**, 054107 (2003).

[55] V. G. Kukhar, N. A. Pertsev, H. Kohlstedt, and R. Waser, Polarization states of polydomain epitaxial $Pb(Zr_{1-x}Ti_x)O^3$ thin films and their dielectric properties, Phys. Rev. B **73**, 214103 (2006).

[56] N. A. Pertsev, A. G. Zembilgotov, and A. K. Tagantsev, Effect of Mechanical Boundary Conditions on Phase Diagrams of Epitaxial Ferroelectric Thin Films, Phys. Rev. Lett. **80**, 1988 (1998).

[57] Anna N. Morozovska, Eugene A. Eliseev, Nicholas V. Morozovsky, and Sergei V. Kalinin, Ferroionic states in ferroelectric thin films, Phys. Rev. B **95**, 195413 (2017).

[58] When deriving the expression, we neglect the intrinsic size effect as well as the term $-d\epsilon_{33}^b/\epsilon_d$ on the right-hand-side, which is possible at $H_{cr} \gg d$.

[59] M. J. Haun, Z. Q. Zhuang, E. Furman, S. J. Jang, and L. E. Cross, Thermodynamic theory of the lead zirconate-titanate solid solution system, part III: Curie constant and sixth-order polarization interaction dielectric stiffness coefficients, Ferroelectrics **99**, 45 (1989).

[60] D. D. Fong, A. M. Kolpak, J. A. Eastman, S. K. Streiffer, P. H. Fuoss, G. B. Stephenson, Carol Thompson, D. M. Kim, K. J. Choi, C. B. Eom, I. Grinberg, and A. M. Rappe, Stabilization of Monodomain Polarization in Ultrathin $PbTiO_3$ Films, Phys. Rev. Lett. **96**, 127601 (2006).

[61] J. Scott Bunch, Arend M. van der Zande, Scott S. Verbridge, Ian W. Frank, David M. Tanenbaum, Jeevak M. Parpia, Harold G. Craighead, and Paul L. McEuen, Electromechanical resonators from graphene sheets, Science **315**, 490 (2007).

[62] N. Levy, S. A. Burke, K. L. Meaker, M. Panlasigui, A. Zettl, F. Guinea, A. H. Castro Neto, and M. F. Crommie,

Strain-induced pseudo-magnetic fields greater than 300 tesla in graphene nanobubbles, Science **329**, 544 (2010).

[63] M. V. Strikha, Non-volatile memory, and IR radiation modulators based upon graphene-on-ferroelectric substrate. A review, Ukr. J. Phys. Opt. **13**, S5 (2012).

[64] According to our estimates, it is several volts and lower depending on the piezoelectric coefficients of the ferroelectric substrate and its thickness.

[65] The very small time of approximately 10^{-12} s required for the piezoresponse is conditioned by acoustic phonons; see, e.g., Ref. [46].

[66] Anatolii I. Kurchak, Anna N. Morozovska, and Maksym V. Strikha, Hysteretic phenomena in GFET: General theory and experiment, J. Appl. Phys. **122**, 044504 (2017).

[67] A. K. Tagantsev and G. Gerra, Interface-induced phenomena in polarization response of ferroelectric thin films, J. Appl. Phys., **100**, 051607 (2006).